DEUTSCHES ELEKTRONEN – SYNCHROTRON DESY

DESY 89-026
March 1989

Periodic-Orbit Sum Rules for the Hadamard-Gutzwiller Model

R. Aurich, F. Steiner
II. Inst. f. Theoretische Physik, Univ. Hamburg

ISSN 0418-9833

NOTKESTRASSE 85 · 2 HAMBURG 52

To be sure that your preprints are promptly included in the
HIGH ENERGY PHYSICS INDEX,
send them to the following address (if possible by air mail):

DESY
Bibliothek
Notkestrasse 85
2 Hamburg 52
Germany

DESY 89-026
March 1989

ISSN 0418 - 9833

Periodic–Orbit Sum Rules for the Hadamard–Gutzwiller Model

by

R.Aurich [1] and F.Steiner

II.Institut für Theoretische Physik , Universität Hamburg
Luruper Chaussee 149 , 2000 Hamburg 50
Federal Republic of Germany

Abstract

It is shown how a variety of periodic–orbit sum rules can be used to extract information about a quantum mechanical system, whose classical counterpart is completely chaotic, from knowledge only of the classical system, and vice versa. The basis is the Selberg trace formula, an exact analogue for the Hadamard–Gutzwiller model of the semiclassical periodic–orbit theory of Gutzwiller, which relates the quantal energies to the lengths of the periodic orbits of the classical system. Statistical properties of the quantal energies in the low energy region are studied, where we restrict ourselves to the level spacing and spectral rigidity.

Submitted to Physica D

[1] Supported by Deutsche Forschungsgemeinschaft under Contract No. DFG–Ste 241/4–1

I Introduction

After three decades of research on classical chaos there is still no clear-cut answer to the question which typical properties betray a quantum mechanical system as one with a *chaotic* classical counterpart. *Quantum chaology* has been defined [1] as the study of semiclassical ($\hbar \to 0$), but non-classical, behaviour characteristic of systems whose classical motion exhibits chaos, i.e. neighbouring trajectories in phase space diverge at an exponential rate and so the time evolution depends infinitesimally on the initial conditions. In quantum mechanics Heisenberg's uncertainty relation prevents an exact determination of the initial conditions in phase space. So one may wonder how a given chaotic system might behave in the transition region between classical and quantum mechanics.

Already in the age of the "old" quantum mechanics Einstein [2] recognized the lack of a substitute for the Bohr–Sommerfeld quantization rules for systems without invariant tori in phase space on which one has to apply these rules. The absence of such tori is a characteristic of chaotic systems. Today the *periodic-orbit theory* is considered to be this substitute for the Bohr–Sommerfeld quantization rules. The periodic-orbit theory was originally derived from semiclassical considerations by Gutzwiller [3] (see also [4–6]) and culminates in an asymptotic *periodic-orbit sum rule* (POSR) which can be written symbolically as

$$\sum(\text{quantal energies}) \approx \sum(\text{classical periodic orbits}) \quad , \quad \hbar \to 0 \quad . \tag{1}$$

(In general, the POSR (1) is at best conditionally convergent. A generalization, that leads to absolutely convergent sum rules, has been worked out recently [7].)

In this paper we consider a conservative Hamiltonian system with two degrees of freedom which is strongly chaotic. Two degrees of freedom are the minimum for a system to be chaotic. In this sense such systems are the simplest ones for the study of manifestations of classical chaos in quantum mechanical systems. The system considered by us is the symmetrical Hadamard–Gutzwiller model [8,9], for which one can derive infinitely many exact POSRs of the type (1). The Hadamard–Gutzwiller model can be considered as a billiard on a surface of negative curvature, which is saddle point shaped everywhere. In contrast to "planar billiards" it has the advantage that the POSRs are mathematically exact relations and not only semiclassical approximations. In the mathematical literature the generalized POSR is known as *Selberg's trace formula*, a deep theorem of harmonic analysis and hyperbolic geometry [10,11]. We shall show that the quantal energies can be determined by the classical periodic orbits with a momentum resolution $\Delta p \sim \frac{2\pi}{l}$, where l is the length of the largest classical periodic orbit taken into account in the sum rule (1). Vice versa, we shall demonstrate that the quantal energies "know" about the length spectrum of the classical periodic orbits. Thus we shall present an exact approach to *quantum chaology of spectra*. A preliminary announcement of our results has already appeared [12].

II The Hadamard–Gutzwiller model

The *Hadamard–Gutzwiller model* is governed by the following classical Lagrangian and Hamiltonian, respectively

$$L = \frac{m}{2} g_{ij} \frac{dx^i}{dt} \frac{dx^j}{dt} \quad , \quad H = \frac{1}{2m} p_i g^{ij} p_j \tag{2}$$

where $p_i = m g_{ij} \frac{dx^j}{dt}$ and $g_{ij} = \frac{4R^2}{(1-x_1^2-x_2^2)^2} \delta_{ij}$ $(i,j = 1,2)$. The dynamical system (2) describes the classical motion (geodesic flow) of a particle of mass m sliding freely on a surface $\mathcal{M}$ of constant negative Gaussian curvature, $K = -\frac{1}{R^2}$, the so-called pseudosphere. In this paper we use the Poincaré disc endowed with the metric g_{ij} as a model for the pseudosphere, where the pseudosphere is mapped into the unit circle on the complex plane: $z = x_1 + ix_2$, $x_1^2 + x_2^2 < 1$. The energy $E = H = L$ is the only constant of motion. There are no invariant tori in phase space, and neighbouring trajectories diverge with time at the rate $e^{\omega t}$, i.e. the classical orbits are unstable, a typical property of chaos. The Liapunov exponent ω is given by $\omega = \sqrt{2E/m}$ (For a recent review, see [13]).

In this paper we consider the simplest case, where the particle moves on a compact Riemannian surface $\mathcal{M}$ of genus 2 and area $A = 4\pi R^2$ which is topologically a double doughnut. In addition, this surface is chosen to possess the highest possible symmetry. In the Poincaré disc, $\mathcal{M}$ is represented by a regular hyperbolic octagon, see fig.2, the fundamental region of a discrete subgroup G of $SU(1,1)/\{\pm 1\}$. (The latter group represents the three-dimensional Lorentz group). The "octagon group" G leads to a tessellation of the pseudosphere in terms of octagons by identifying the points z and z', where $z' = bz$ and $b \in G$. The tessellation can be viewed as cutting out a piece of the whole pseudosphere and gluing together opposite edges, which then leads to the imagination of a double doughnut. On the Poincaré disc, the boosts $b \in G$ can be represented by 2×2 matrices

$$b = \begin{pmatrix} \alpha & \beta \\ \beta^* & \alpha^* \end{pmatrix} \quad , \quad |\alpha|^2 - |\beta|^2 = 1 \quad , \quad |\mathrm{Tr}\, b| > 2 \quad ,$$

and their action on a point z is defined by the linear fractional transformation

$$z' = bz = \frac{\alpha z + \beta}{\beta^* z + \alpha^*} \quad ,$$

where every product of boosts b_i's corresponds to the product of their representing matrices. To construct the regular octagon one has to choose the four generators b_k , $k = 1, 2, 3, 4$, of the "octagon group" G with

$$\alpha_k = \cosh \frac{l_0}{2} = 1 + \sqrt{2} \qquad \text{and} \qquad \beta_k = e^{i\frac{k\pi}{4}} \sinh \frac{l_0}{2} \quad ,$$

where l_0 denotes the length of the shortest periodic orbit. One can associate a periodic orbit with each boost $b \in G$, whose length $l(b)$ is given by [14]

$$l(b) = 2 \,\mathrm{arcosh}\, |\mathrm{Tr} b| \quad . \tag{3}$$

This is a very important relation for the calculation of the length spectrum of periodic orbits.

The quantum mechanics of the Hadamard–Gutzwiller model is determined by the *Schrödinger equation*

$$-\frac{\hbar^2}{2mR^2} \Delta \Psi_n(z) = E_n \Psi_n(z) \tag{4}$$

where $\Delta = g^{-1/2} \partial_i (g^{1/2} g^{ij} \partial_j)$ is the Laplacian on $\mathcal{M}$, $g = \det(g_{ij})$. Eq.(4) has to be solved with *periodic boundary conditions*, i.e. $\Psi_n(bz) = \Psi_n(z)$ for all $b \in G$. There is then only a discrete energy spectrum $\{E_n\}$ with a non-degenerate zero mode: $0 = E_0 < E_1 < E_2 < \cdots$. A possible degeneracy of the quantal energy E_n is denoted by $d_n \in \mathbf{N}$. For $n \to \infty$ we have $E_n \sim \frac{4\pi}{A} n$ (Weyl's law), if $d_n = 1$ for all n. Since the eigenvalues scale as $E_n = \frac{\hbar^2}{2mR^2} \lambda_n$, where λ_n is dimensionless and independent of $\hbar, m$ and R, we use from now on the following *units* : $\hbar = 2m = R = 1$. Then the Schrödinger equation simply reads

$$-\Delta \Psi_n(z) = E_n \Psi_n(z) \qquad \text{with} \qquad \Delta = \frac{1}{4}(1 - x_1^2 - x_2^2)^2 \left(\frac{\partial^2}{\partial x_1^2} + \frac{\partial^2}{\partial x_2^2} \right) \quad . \tag{5}$$

III The length spectrum

The length spectrum $\{l_n\}$ of the periodic orbits in the regular octagon is of crucial importance as the "classical" input in the Selberg trace formula which will be discused in section V. The computation and some surprising properties of the length spectrum $\{l_n\}$ have already been presented in [14]. Here we only mention that we calculated the length spectrum by computing the conjugacy classes of the "octagon group" G and then used eq.(3) which yields the connection between a group element $b \in G$

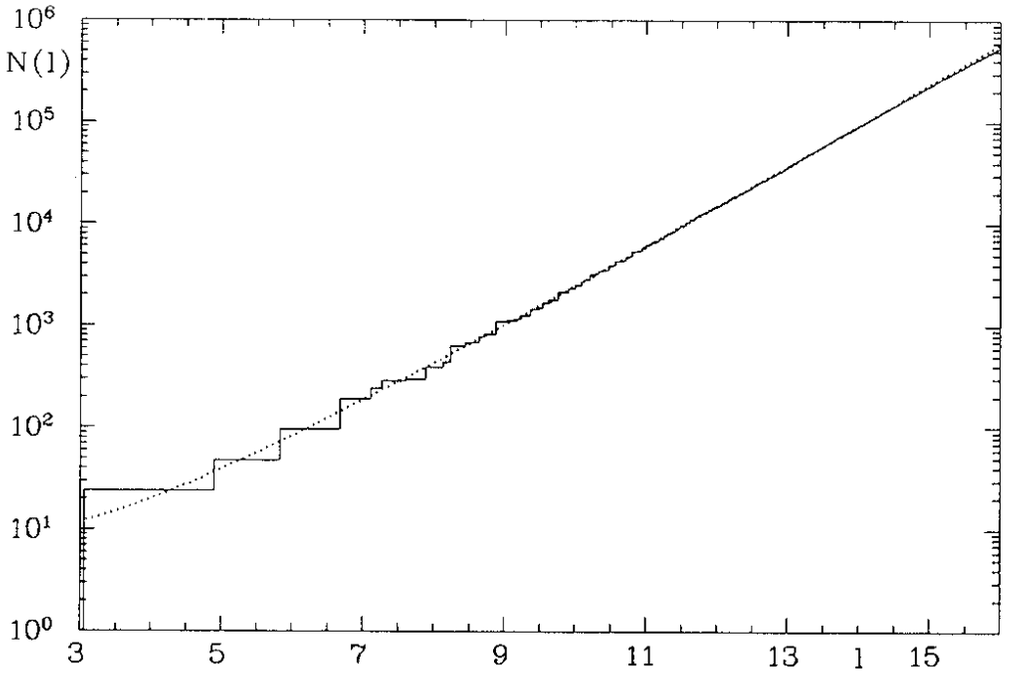

Figure 1: Huber's asymptotic law, eq.(6), (dotted line) is shown in comparison with the staircase function $N(l)$

and the length of its associated periodic orbit. The length spectrum $\{l_n\}$ proliferates exponentially according to *Huber's law* [15] which is typical for chaotic systems

$$N(l) \sim \frac{e^l}{l}\left(\sum_{n=0}^{M}\frac{n!}{l^n} + O(l^{-M-1})\right) \quad , \; l \to \infty \tag{6}$$

where

$$N(l) := \sum_{l_n \le l} g_n \quad ; \; g_n \text{ is the multiplicity of the length } l_n \; . \tag{7}$$

Figure 1 shows the staircase function $N(l)$ in comparison with Huber's law, where we have taken into account correction terms up to $M = 3$. The figure reveals that the spectrum is nearly completely known up to lengths of order 14.5. In principle we are able to compute even more lengths, but the computer time increases very rapidly with increasing lengths. This is a consequence of Huber's law: the exponential proliferation of long lengths forces one to be content with this computed length spectrum. Nevertheless, it already suffices to yield very important results as will be discussed in sect.V.

IV The energy spectrum

Now let us turn to the numerical solution of the Schrödinger equation (5). There exist various computational methods to solve a partial differential equation like eq.(5). The special difficulty in solving our problem are the periodic boundary conditions as described in section II. These boundary conditions can be incorporated in the two well elaborated methods of finite differences and finite elements. We have chosen the latter one because of its higher flexibility. In this method one can describe more easily curved boundaries as they occur in our model. Here we only give a short description of the method of finite elements because there exists an extensive literature on this subject.

The method of finite elements is based on the variational principle, which in our case states that

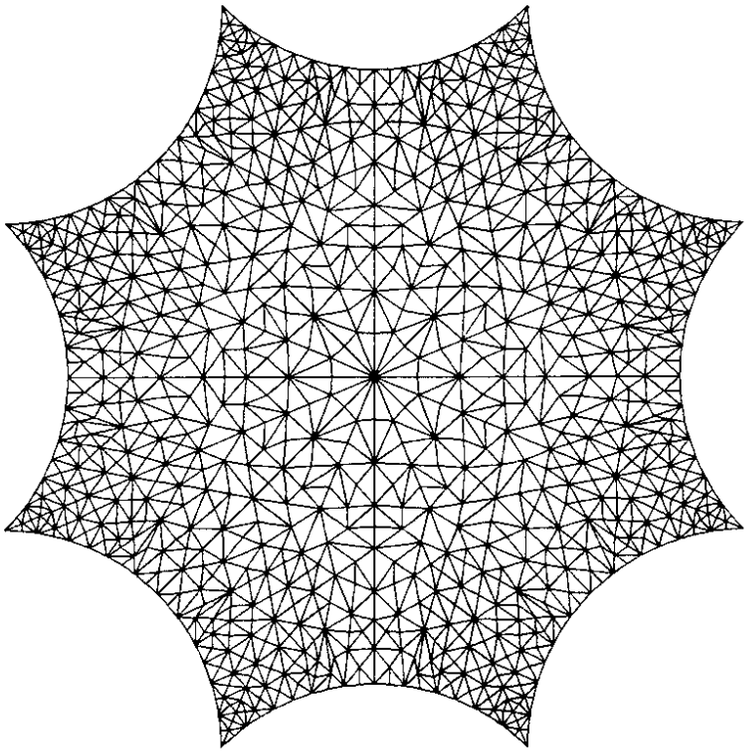

Figure 2: The tessellation of the fundamental domain is depicted which is used for the method of finite elements. It leads to matrices of dimension 3518 if one uses ansatz–functions of second order in the triangles.

an eigenfunction Ψ of the equation

$$\frac{\partial^2\Psi}{\partial x_1^2} + \frac{\partial^2\Psi}{\partial x_2^2} + \frac{4E}{(1-x_1^2-x_2^2)^2}\Psi = 0 \tag{8}$$

minimizes the variational integral

$$I = \int\int_{octagon} \left\{ \left(\frac{\partial\Psi}{\partial x_1}\right)^2 + \left(\frac{\partial\Psi}{\partial x_2}\right)^2 - \frac{4E}{(1-x_1^2-x_2^2)^2}\Psi^2 \right\} dx_1\, dx_2 \quad . \tag{9}$$

To evaluate this integral the fundamental domain is tessellated by finite elements (fig.2) for which we choose triangles. On each triangle Ψ is approximated by a polynomial of low order. In the following description we restrict ourselves to polynomials of second order, where the ansatz reads as

$$\Psi(x_1,x_2) = c_{1,\epsilon} + c_{2,\epsilon}x_1 + c_{3,\epsilon}x_2 + c_{4,\epsilon}x_1^2 + c_{5,\epsilon}x_1x_2 + c_{6,\epsilon}x_2^2 \tag{10}$$

with distinct coefficients $c_{i,\epsilon}$ on each element ϵ. The ansatz (10) must be continuous on adjacent elements which connects the coefficients $c_{i,\epsilon}$ of an element with the corresponding $c_{i,\epsilon'}$'s of the neighbouring elements. This is accomplished by expressing the 6 coefficients $c_{i,\epsilon}$ by the 6 values u_i which Ψ takes at the corners and the centres of the edges of the triangle. The ansatz function along an edge is then uniquely determined by the three values u_i belonging to this edge. Therefore the function is continuous between neighbouring triangles because they share the common edge points u_i.

Then one goes into eq.(9) which yields a generalized eigenvalue problem

$$A\vec{u} \;=\; E\; B\vec{u} \tag{11}$$

where A and B are real symmetric matrices and in addition B is positive definite. The vector $\vec{u}$ consists of the values u_i of Ψ at the boundary of the triangles. The eigenvalue problem (11) is solved by a standard NAG-routine.

In table 1 we list the first 100 eigenvalues which are calculated at the HLRZ Jülich on a CRAY X-MP. In this calculation the matrices A and B have the dimension 3518 where we used the polynomial (10) as the ansatz-function in the triangles. In this table the last figure of the eigenvalues may be a bit too high, because our variational procedure yields upper bounds for the eigenvalues.

E_i	d_i	note on the group	E_i	d_i	note on the group
0	1	ϑ_1^1	50.55	3	ϑ_4^1
3.8388	3	ϑ_1^1	57.59	4	
5.353	4		59.58	4	
8.249	2	ϑ_1^1 and ϑ_3^1	61.02	2	ϑ_1^1 and ϑ_3^1
14.728	4		62.63	3	ϑ_3^1
15.048	3	ϑ_4^1	67.61	3	ϑ_1^1
18.658	3	ϑ_1^1	71.59	4	
20.526	4		73.66	2	ϑ_2^1 and ϑ_4^1
23.078	1	ϑ_1^1	74.92	1	ϑ_1^1
28.079	3	ϑ_3^1	75.53	3	ϑ_4^1
30.850	4		75.9	4	
32.673	1	ϑ_4^1	86.4	4	
36.238	2	ϑ_1^1 and ϑ_3^1	86.7	3	ϑ_1^1
39.00	4		91.4	1	ϑ_3^1
40.11	3	ϑ_2^1	93.8	4	
42.90	4		97.8	3	ϑ_2^1
44.01	3	ϑ_1^1	100.7	3	ϑ_4^1

Table 1: The first 100 eigenvalues of the regular octagon

Fig.3 shows the *staircase function*

$$N(E) = \#\{E_n | E_n \leq E\} \tag{12}$$

in comparison with *Weyl's law* $N(E) \sim E, E \to \infty$. As can be seen the asymptotic law describes well the staircase down to the smallest eigenvalues.

Most of the eigenvalues are degenerated, as a close look on table 1 reveals (d_i denotes the degeneracy of level E_i). At first sight this seems to be incompatible with the expected "level repulsion" for quantum systems with a classical chaotic counterpart. But these degeneracies are due to the symmetry the system possesses as will be explained in section VI. The column "note on the group" describes the membership of an eigenvalue to a one-dimensional group representation as will be explained in section VI too. The remaining eigenvalues belong to two-dimensional representations.

V Periodic–orbit sum rules

V.1 The Selberg trace formula

The Selberg trace formula [10,11] is an exact relation between the classical length spectrum $\{l_n\}$ of the periodic orbits and the quantum mechanical energy spectrum $\{E_n\}$. If one expresses the energy

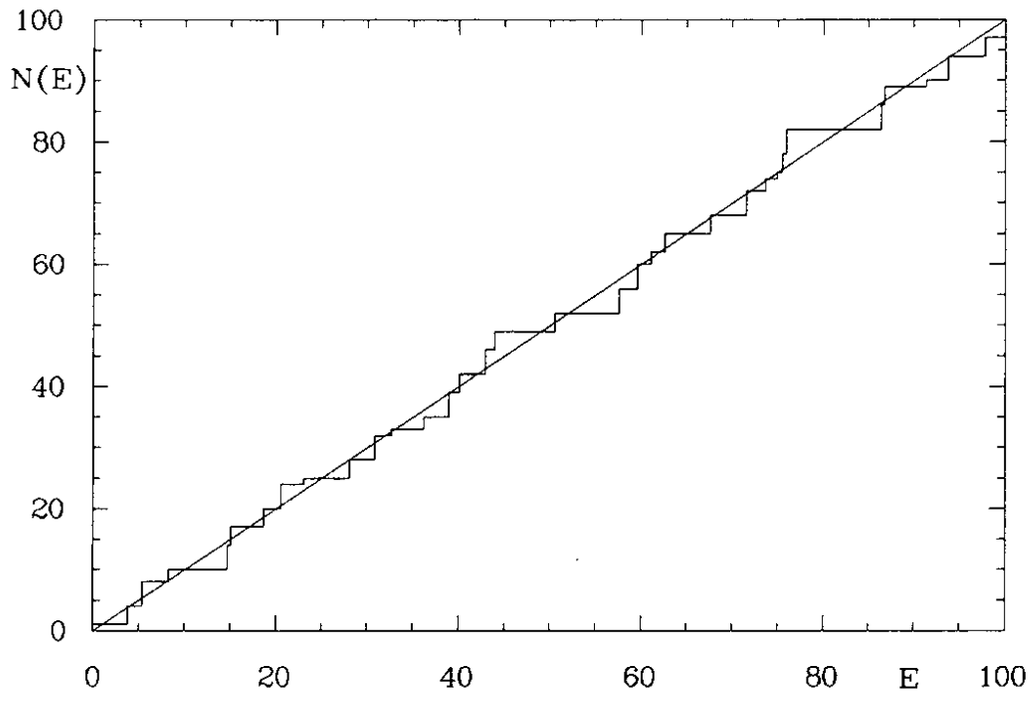

Figure 3: The staircaise function $N(E)$ is shown in comparison with Weyl's law $N(E) \sim E$, $E \to \infty$.

E_n by the momentum p_n via $E_n = \frac{1}{4} + p_n^2$ than the *Selberg trace formula* can be written as

$$\sum_{\{p_n\}} d_n \, h(p_n) \;=\; \frac{\mathrm{Area}(F)}{4\pi} \int_{-\infty}^{\infty} dp \, p \, \tanh(\pi p) \, h(p) \;+\; \sum_{\{l_n\}} \sum_{k=1}^{\infty} \frac{g_n \, l_n}{2 \sinh \frac{k \, l_n}{2}} \, g(k \, l_n) \qquad (13)$$

where $\{l_n\}$ denotes a summation over all primitive periodic orbits with length l_n ordered as $0 < l_0 < l_1 < l_2 < \ldots$ and associated multiplicities g_n, whereas the k-summation counts multiple traversals corresponding to periodic orbits of length $kl_n, k \geq 1$. The multiplicities of p_n are denoted by d_n and $g(x)$ is the Fourier transform of $h(p)$:

$$g(x) = \frac{1}{\pi} \int_0^{\infty} dp \, \cos(xp) \, h(p) \quad . \qquad (14)$$

To ensure the absolute convergence of the series and the integral in eq.(13) $h(p)$ must obey the following three restrictions:

- $h(p)$ is even : $h(p) = h(-p)$
- $h(p)$ is holomorphic in the strip $|\ \mathrm{Im}\ p| \leq \frac{1}{2} + \varepsilon \ \ ; \ \ \varepsilon > 0$
- $|h(p)| \leq a(1 + |p|^2)^{-1-\varepsilon} \quad (a > 0)$ in this strip.

This formula is the basis of the perodic–orbit theory which yields infinitely many periodic–orbit sum rules (POSRs). An analogous formula can be found for general systems, chaotic or not, but it is then only semiclassically valid [3–7], i.e. there are unknown correction terms of order $\hbar^2$. In contrast in our case of compact Riemann surfaces of constant negative curvature this relation is exact. This makes it possible to study the POSRs even with an incompletely known length spectrum. Knowing only part of the length spectrum is a handicap common to almost all applications of periodic–orbit theory. In other physical systems this is somewhat troublesome because there the formulas are only semiclassically

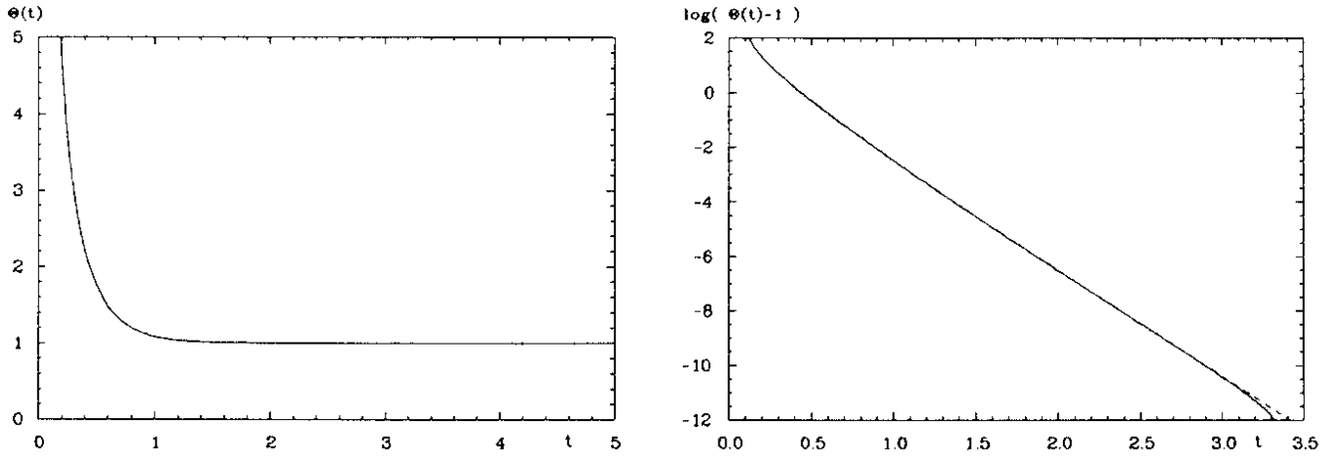

Figure 4: The heat kernel $\Theta(t)$ is computed using the lenght spectrum (full line) and using the first 115 eigenvalues (dashed line)

valid, i.e. either one needs very high eigenvalues of the corresponding Schrödinger equation, which are very hard to obtain, or one has to cope with low eigenvalues but then the unknown correction terms of order $\hbar^2$ may be important.

In the following subsections we discuss various functions $h(p)$ constructed for different applications.

V.2 The heat kernel

As our first example of an exact POSR let us consider the trace of the *heat kernel* (partition function) defined by $\Theta(t) = \mathrm{tr}(e^{-\hat{H}t})$, $\hat{H} = -\Delta, t > 0$. For this application we have to use

$$h(p) \;=\; e^{-(\frac{1}{4}+p^2)\,t} \;=\; e^{-E\,t} \quad . \tag{15}$$

Then the Selberg trace formula yields

$$\Theta(t) = \sum_{n=0}^{\infty} d_n e^{-E_n t} = \frac{\mathrm{Area}(F)\; e^{-t/4}}{(4\pi t)^{3/2}} \int_0^\infty db\; \frac{b\; e^{-\frac{b^2}{4t}}}{\sinh\frac{b}{2}} + \frac{e^{-\frac{t}{4}}}{4\sqrt{\pi t}} \sum_{\{l_n\}} \sum_{k=1}^{\infty} \frac{g_n l_n}{\sinh\frac{k l_n}{2}} e^{-\frac{(k l_n)^2}{4t}} \quad , \tag{16}$$

where we have used

$$\tanh(\pi p) = \frac{1}{\pi} \int_0^\infty db\; \frac{\sin(pb)}{\sinh\frac{b}{2}} \quad . \tag{17}$$

It follows from Selberg's theorem that the PO sum in (16) converges absolutely. This can also be seen directly from the fact that the exponential proliferation of the length spectrum (see eq.(6)) is compensated nicely by the Gaussian suppression factor in eq.(16). Fig.4a shows the heat kernel obtained from the length spectrum $\{l_n\}$ (full line) using the first 200000 lengths and from the eigenvalue spectrum $\{E_n\}$ (dashed line). The small-t behaviour of the heat kernel $\Theta(t)$ is determined by the integral term in eq.(16) and is given by (the coefficients b_m are explicitly known, see [11])

$$\frac{\mathrm{Area}(F)\; e^{-t/4}}{(4\pi t)^{3/2}} \int_0^\infty db\; \frac{b\; e^{-\frac{b^2}{4t}}}{\sinh\frac{b}{2}} \;=\; \frac{1}{t} \sum_{m=0}^{N} b_m t^m + O(t^N) \quad . \tag{18}$$

Reinsertion of $\hbar$ in eq.(16) can be accomplished by the replacement $t \to \hbar t$. Thus the semiclassical limit ($\hbar \to 0$) corresponds to the limit $t \to 0$ ($E_n \to \infty$). It then follows that Θ diverges as $(\hbar t)^{-1}$ from

which one derives immediately Weyl's law. The terms $b_m(\hbar t)^m, m \geq 1$, correspond to semiclassical perturbation theory, i.e. to an asymptotic expansion in $\hbar$ analogous to higher WKB approximations in the case of non-chaotic systems. In addition, the PO sum (16) contains an infinite number of terms proportional to $\exp[-\frac{(kl_n)^2}{4\hbar t}]$ which are entirely of non-perturbative nature. The crucial point to notice is that by eq.(16) one has succeeded in summing up not only perturbation theory but also all non-perturbative contributions.

While the small-t behaviour of $\Theta(t)$ corresponds to the semiclassical limit, the large-t behaviour gives us information on the ground state and low excited levels according to $\Theta(t) \simeq 1+d_1 e^{-E_1 t} (t \to \infty)$. In fig. 4b we have plotted the function $\ln[\Theta(t) - 1]$ for $0 < t < 3.5$ as obtained from the r.h. side of eq.(16) using the first 200000 lengths. One observes a strong exponential fall off as expected. From a fit we obtain $E_1 = 3.83$ assuming $d_1 = 3$ in nice agreement with our results from finite elements. The main conclusion to be drawn from fig. 4b is that there are no *"small" eigenvalues* (apart from the ground state $E_0 = 0$) which are defined by $0 < E_n \leq \frac{1}{4}$ ($\hat{=} \frac{\hbar^2}{8mR^2}$). The question of "small" eigenvalues is of great importance for number theory. In our special case of the octagon group the exclusion of "small" eigenvalues implies that the analogue of the Riemann hypothesis is true for the Selberg zeta function $Z(s)$ defined in eq.(20) below. By the very definition of the heat kernel it is clear that $\Theta(t)$ is a monotonously decreasing function of t and thus by itself not suitable to show any direct signature of chaos. (See, however, the "modulated heat kernel" defined in eq.(30) below.)

V.3 The resolvent and Selberg's zeta function

Another spectral function of great importance in quantum mechanics is the energy-dependent *Green's function* (resolvent). We start with

$$h(p) = \frac{1}{p^2 + (\sigma - \frac{1}{2})^2} - \frac{1}{p^2 + (s - \frac{1}{2})^2} = \frac{1}{s(1-s) - E} - \frac{1}{\sigma(1-\sigma) - E} \quad , \tag{19}$$

which is an admissible function in the Selberg trace formula for $\mathrm{Re}\sigma > 1$ and $\mathrm{Re}s > 1$. The trace formula can be conveniently expressed by the *Selberg zeta function* which for $\mathrm{Re}s > 1$ is defined in analogy to the Riemann zeta function $\zeta(s)$ by the following Euler product over the length spectrum $\{l_n\}$

$$Z(s) = \prod_{\{l_n\}} \prod_{k=0}^{\infty} \left[1 - e^{-(s+k)l_n}\right]^{g_n} \quad . \tag{20}$$

$Z(s)$ is an entire function of s whose non-trivial zeros at $s = s_n := \frac{1}{2} \pm ip_n$ ($n \geq 1$) are exactly given by the momenta p_n related to the quantal energies by $E_n = p_n^2 + \frac{1}{4} = s_n(1 - s_n)$. (We define $p_0 = \frac{i}{2}$, $p_n > 0$ for $n = 1, 2, \cdots$). Thus $\frac{Z'(s)}{Z(s)}$ is a meromorphic function of s whose non-trivial poles are located exactly at the quantal energies E_n. The Selberg trace formula yields for $h(p)$ of eq.(19)

$$\sum_{n=0}^{\infty} d_n \left[\frac{1}{s(1-s) - E_n} - \frac{1}{\sigma(1-\sigma) - E_n}\right] = \frac{\mathrm{Area}(F)}{2\pi} [\Psi(s) - \Psi(\sigma)] - \frac{1}{2s-1}\frac{Z'(s)}{Z(s)} + \frac{1}{2\sigma - 1}\frac{Z'(\sigma)}{Z(\sigma)} \tag{21}$$

where $\Psi(s) = \frac{\Gamma'(s)}{\Gamma(s)}$ is the digamma function. Isolating the ground state $E_0 = 0$,

$$\frac{1}{s(1-s)} + \sum_{n=1}^{\infty} d_n \left[\frac{1}{s(1-s) - E_n} - \frac{1}{\sigma(1-\sigma) - E_n}\right] = \frac{\mathrm{Area}(F)}{2\pi} [\Psi(s) - \Psi(\sigma)] - \frac{1}{2s-1}\frac{Z'(s)}{Z(s)} + \frac{1}{2\sigma-1}\frac{Z'(\sigma)}{Z(\sigma)} + \frac{1}{\sigma(1-\sigma)} \quad , \tag{22}$$

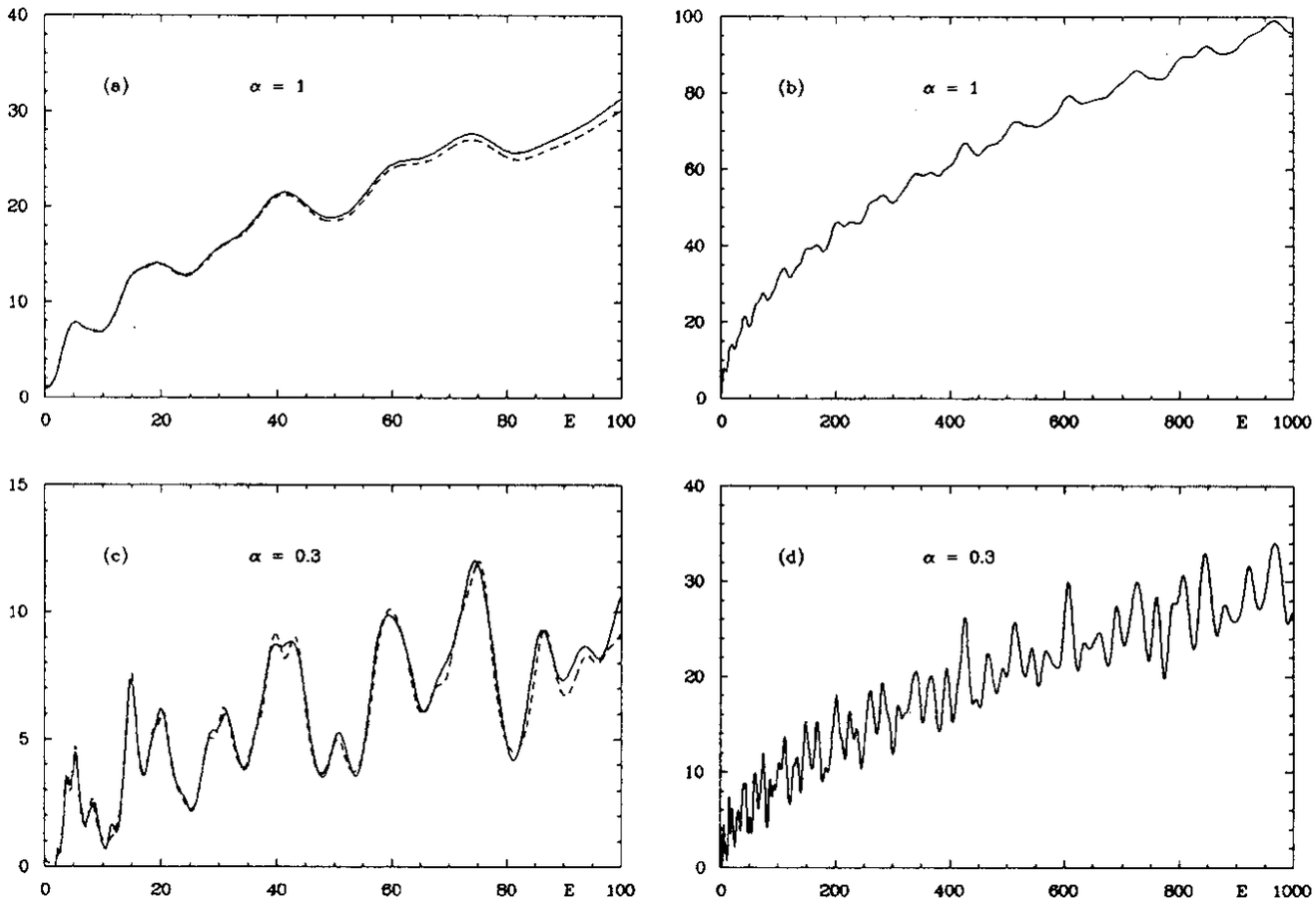

Figure 5: The Breit–Wigner smeared level density is shown as explained in the text

one can eliminate σ by taking the limit $\sigma \to 1+$ because the limit

$$\lim_{\sigma \to 1+} \left[\frac{1}{2\sigma - 1} \frac{Z'(\sigma)}{Z(\sigma)} + \frac{1}{\sigma(1-\sigma)} \right] = \frac{1}{2} \frac{Z''(1)}{Z'(1)} - 1 := \gamma_\Delta + \frac{\mathrm{Area}(F)}{2\pi} \Psi(1) \tag{23}$$

exists where we have defined the so-called generalized Euler constant γ_Δ. (For the regular octagon we obtain $\gamma_\Delta = -0.595\cdots$.) Finally we arrive [11] at the following sum rule for the regularized trace of the Green's function expressed in terms of the logarithmic derivative of $Z(s)$ ($E = s(1-s)$)

$$\frac{1}{E} + \sum_{n=1}^{\infty} d_n \left[\frac{1}{E - E_n} + \frac{1}{E_n} \right] = \gamma_\Delta + \frac{\mathrm{Area}(F)}{2\pi} \Psi(s) - \frac{1}{2s-1} \frac{Z'(s)}{Z(s)} \quad . \tag{24}$$

Unfortunately at present this sum rule cannot be used to determine the eigenvalues E_n by searching for the poles of the r.h.side of eq.(24), i.e. the non–trivial zeros of $Z(s)$, because they occur on the critical line $\mathrm{Re}\, s = \frac{1}{2}$ where the Euler product (20) diverges. What is lacking is an analogue of the Riemann–Siegel formula which would allow an analytic continuation of $Z(s)$ to the critical line.

V.4 The Breit–Wigner smeared level density

A formula which can be used to locate the eigenvalues E_n can be derived from eq.(24) nevertheless. The possible way out is to work with a *smeared Green's function* which can be obtained from eq.(24) by making the replacement $E \to E + i\alpha\sqrt{E}$ ($E > \frac{1}{4}, \alpha > 1$) and then taking the imaginary part of both sides of the equation. Then we end up with the following exact (and convergent !) POSR for

the *smeared spectral density*

$$\sum_{n=0}^{\infty} \frac{\alpha^2 E d_n}{(E-E_n)^2+\alpha^2 E} = -2\alpha\sqrt{E}\ \mathrm{Im}\ \Psi(\frac{1}{2}+A_- - iA_+) + \frac{\alpha\sqrt{E}}{4(A_+^2+A_-^2)} \sum_{\{l_n\}} \sum_{k=1}^{\infty} \frac{g_n l_n \epsilon^{-A_- k l_n}}{\sinh \frac{k l_n}{2}} [A_+ \cos(A_+ k l_n) + A_- \sin(A_+ k l_n)] \quad (25)$$

where $A_\pm = 2^{-1/2}\{\sqrt{(E-\frac{1}{4})^2+\alpha^2 E} \pm E \mp \frac{1}{4}\}^{1/2}$. The l.h. side of eq.(25) is a sum over "Breit–Wigner resonances" with individual maxima at $E = E_n$ and maximum values equal to the degeneracies d_n. Unfortunately one has to choose an energy–dependent smearing $\alpha\sqrt{E}$, because an energy–independent smearing would result in a divergent POSR.

In figs. 5a,c we show the smeared spectral density (25) for $E \leq 100$ choosing $\alpha = 1$ and $\alpha = 0.3$, respectively. The r.h. side of eq.(25) has been computed using 200000 primitive orbits (full line), whereas the l.h. side has been obtained from the first 115 quantal energies (dashed line). The agreement is impressive. In fig. 5b,d we show our evaluation of the r.h. side of eq.(25) in a very large energy range extending up to $E = 1000$ using again $\alpha = 1$ and $\alpha = 0.3$. The graphs shown in figs. 5a–d show a bumpy structure, as expected. Since the energy resolution goes as $\Delta E \sim \alpha\sqrt{E}$, it is clear that for $\alpha > 1$ the Breit–Wigner smeared spectral density is too coarse and therefore not well adopted for calculating individual levels. The situation improves if α can be made smaller than the critical value 1, assuming that the series are still conditionally convergent. Figs. 5c,d show, indeed, that the resolution becomes better if α is lowered from 1 to 0.3. The spectral function (25) gives a collective property of the quantal spectrum, namely a clustering with scale ΔE. For $\alpha = 0.3$ (fig. 5c) one sees a close correlation between the bumps obtained from the periodic orbits and the quantal energies.

To keep things as simple as possible, let us discuss in more detail only the critical value $\alpha = 1$, as in figs. 5a,b. It is easy to see that in this case the r.h. side of (25) requires the knowledge of the Selberg zeta function at $s = 1 - i\sqrt{E}$, i.e. $Z(1-i\sqrt{E})$ (see eq.(24)). Thus the chaos in the motion of the particle manifests itself in the dependence of the Selberg zeta function on the energy. The graphs shown in fig. 5 look totally unpredictable and their explicit calculation is certainly quite difficult for large values of E. This is just what is expected in view of the number–theoretical similarity between $Z(s)$ and the Riemann zeta function $\zeta(s)$.

V.5 The Gaussian smeared level density

There remains the challenge to find a method which allows us to make the scale ΔE smaller and smaller until eventually all details of the quantal spectral density can be obtained (at least in principle) by summing classical periodic orbits. The smeared spectral density of the previous subsection has the disadvantage that *absolute* convergence can only be proved for $\alpha > 1$, i.e. for $\alpha < 1$ one must compare the curve obtained from the length spectrum with that from the eigenvalue spectrum to be sure that the sum rule works even for $\alpha < 1$. Nevertheless, one can arrive at a POSR which is absolutely convergent for an arbitraryly small smearing parameter, if one uses a *Gaussian* instead of a Breit–Wigner *smearing*. Inserting

$$h(p') = e^{-\frac{(p'-p)^2}{\epsilon^2}} + e^{-\frac{(p'+p)^2}{\epsilon^2}} \quad (26)$$

in eq.(13) one arrives at

$$\sum_{n=0}^{\infty} d_n \left[e^{-\frac{(p-p_n)^2}{\epsilon^2}} + e^{-\frac{(p+p_n)^2}{\epsilon^2}}\right] = 2\int_0^\infty dp'\, p'\, \tanh(\pi p') \left[e^{-\frac{(p'-p)^2}{\epsilon^2}} + e^{-\frac{(p'+p)^2}{\epsilon^2}}\right] + \frac{\epsilon}{2\sqrt{\pi}} \sum_{\{l_n\}} \sum_{k=1}^{\infty} \frac{g_n l_n}{\sinh \frac{k l_n}{2}} \cos(p k l_n) e^{-\frac{\epsilon^2}{4}(k l_n)^2} \quad . \quad (27)$$

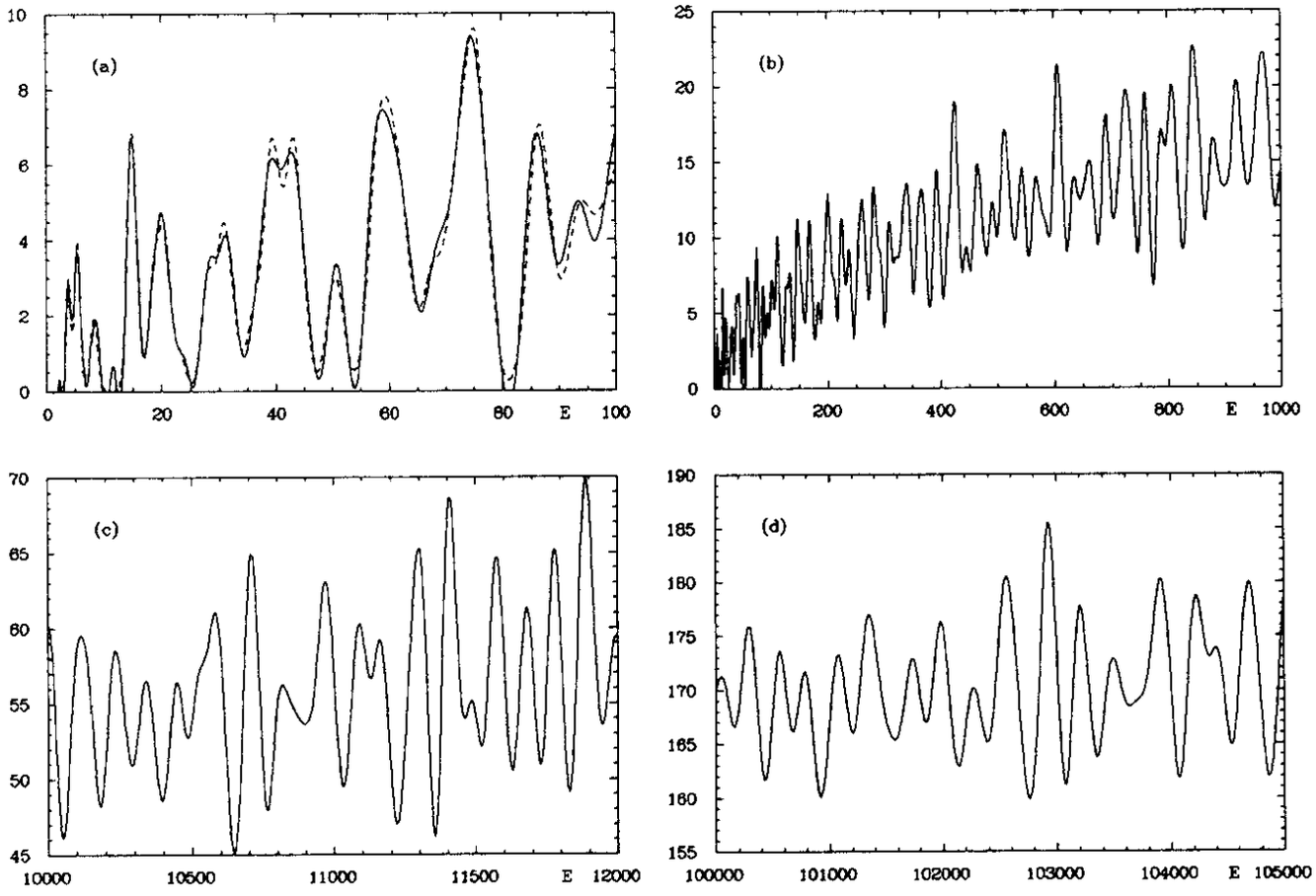

Figure 6: The Gaussian smeared level density is shown as explained in the text

Here $p = \sqrt{E - \frac{1}{4}} > 0$ denotes the momentum. It follows from Selberg's theorem that all series and the integral in the POSR (27) converge absolutely for any $\epsilon > 0$.

For small ϵ the l.h. side of eq.(27) represents a series of delta–like functions of width $\Delta p \sim \sqrt{2\epsilon}$ having peaks at the exact level positions $p = p_n$ $(n \geq 1)$ and ϵ–independent height d_n. Away from the maximum of the peaks the curve declines exponentially as can be read off from eq.(27) in contrast to the Breit–Wigner smeared level density where the fall off is only $\frac{1}{E}$. If ϵ is made smaller, more and more terms in the sum over classical orbits on the r.h. side of (27) contribute with faster oscillations until eventually they sum up in a magic conspiracy to give peaks at the quantal energies. Each periodic orbit b contributes an oscillation to the smeared spectral density which has a "wave length" $\Delta p \sim \frac{2\pi}{l(b)}$, which implies that a resolution of order $\Delta p \sim \sqrt{2\epsilon}$ requires a summation over the length spectrum up to lengths of order $l(b) \sim \frac{\sqrt{2}\pi}{\epsilon} \simeq 29$ for $\epsilon = 0.15$. In fig. 6b we show the *Gaussian level density* (27) for $\epsilon = 0.15$ as a function of the energy E for $E \leq 1000$ taking into account the first 200000 primitive periodic orbits corresponding to $l(b) \leq 28.6275$. Fig. 6a shows the same result at low energies in comparison with the result computed from the first 115 quantal energies as obtained from our finite element method (dashed line). The agreement between the two results is excellent. One sees beautiful peaks at the quantal energies which can be read off directly with an energy resolution $\Delta E = 2p\ \Delta p$ from figs. 6a,b together with their degeneracies. (At finer scales, the degeneracies may dissolve in near–degeneracies.) In figs. 6c,d we present the smeared level density for very large energy ranges for which is no realistic hope to get the eigenvalues from a direct solution of the Schrödinger

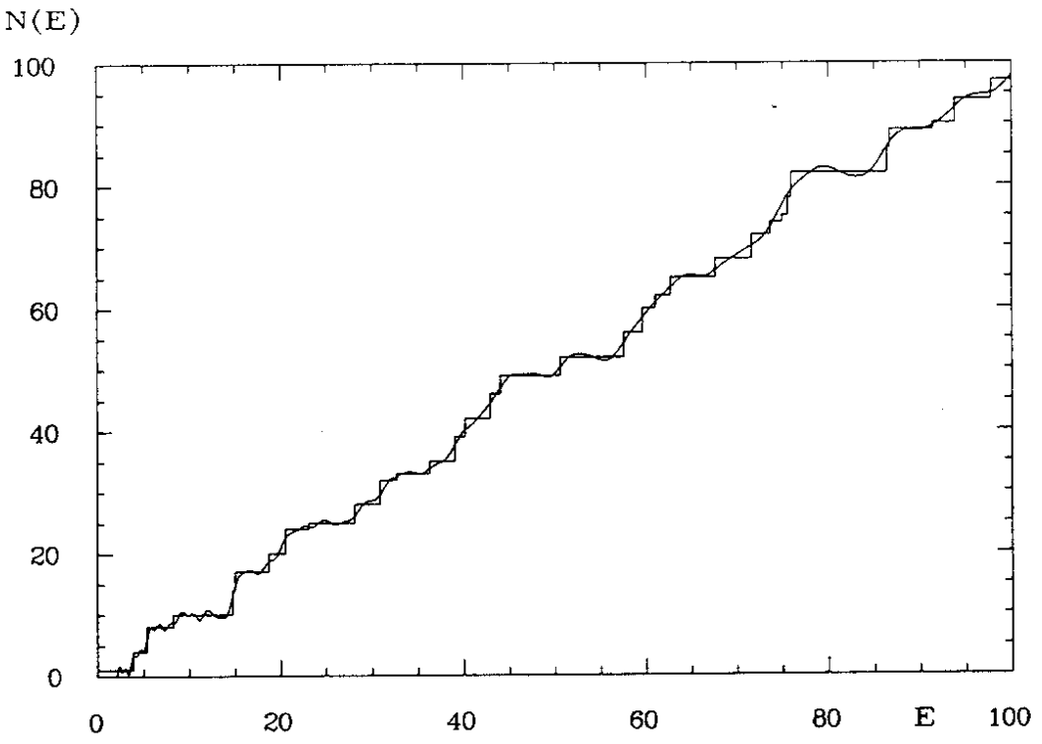

Figure 7: The smoothed staircase $N_\epsilon(E)$, eq.(28), is shown in comparison with the "true" staircase function $N(E)$ obtained from the quantal energies

equation. The resolution of the peaks is somewhat coarser in this case as explained above, but the unpredictable behaviour of the curves seems to be the same.

In order to illustrate the crucial role played by the multiplicities $\{g_n\}$ of the length spectrum $\{l_n\}$, we have evaluated the POSR (27) taking into account the first 10000 primitive periodic orbits with the exact lengths but replacing g_n by the mean value $8\sqrt{2}e^{l_n/2}/l_n$, as derived in [14]. It turns out that the nice agreement for the Gaussian level density (27) is destroyed, since one obtains a graph which shows very large but regular oscillations, i.e. the chaotic peaks seen in fig. 6 are completely washed out.

V.6 The smoothed staircase

The staircase function $N(E)$ can be obtained from eq.(27), too:

$$\begin{aligned} N(E) &= 1 + \int_{1/4}^{E} dE' \sum_{n=1}^{\infty} d_n\, \delta(E' - E_n) \\ &= 1 + \int_0^{\sqrt{E-\frac{1}{4}}} dp' \sum_{n=1}^{\infty} d_n\, \left[\delta(p' - p_n) + \delta(p' + p_n)\right] \\ &= 1 + \lim_{\epsilon\to 0} \sum_{n=1}^{\infty} d_n \int_0^{\sqrt{E-\frac{1}{4}}} dp'\, f_\epsilon(p', p_n) \quad \text{with} \quad f_\epsilon(p', p'') = \frac{1}{\sqrt{\pi}\epsilon}\left\{ e^{-\frac{(p'-p'')^2}{\epsilon^2}} + e^{-\frac{(p'+p'')^2}{\epsilon^2}} \right\}, \end{aligned}$$

where the 1 arises from the zero-mode. For $\epsilon > 0$ we get a *smoothed staircase function* $N_\epsilon(E)$ with $\lim_{\epsilon\to 0} N_\epsilon(E) = N(E)$ and $(E > \frac{1}{4})$

$$\begin{aligned} N_\epsilon(E) &= \frac{4}{\sqrt{\pi}\epsilon} \int_0^{\infty} dp''\, p'' \tanh \pi p'' \int_0^{\sqrt{E-\frac{1}{4}}} dp'\, \cosh \frac{2p'p''}{\epsilon^2}\, e^{-\frac{p'^2+p''^2}{\epsilon^2}} \\ &\quad + \frac{1}{2\pi} \sum_{\{l_n\}} \sum_{k=1}^{\infty} \frac{g_n \sin(\sqrt{E-\frac{1}{4}}\, k\, l_n)}{k \sinh \frac{k\, l_n}{2}}\, e^{-\left(\frac{\epsilon\, k\, l_n}{2}\right)^2} . \end{aligned} \tag{28}$$

The result of the numerical evaluation is shown in fig. 7 in comparison with the "true" staircase obtained from the quantal energies. We have used $\epsilon = 0.05$, a value which is too small to yield an accurate curve for the Gaussian level density. However, in the case of $N_\epsilon(E)$ it leads to a reasonable approximation because here the integration smoothes the non–physical oscillations, which occur in the case of too low ϵ's in the smeared Gaussian level density.

V.7 The cosine–modulated heat kernel

In the preceding subsections the main question was how one can extract the locations of the eigenvalues from the length spectrum $\{l_n\}$. But one can reverse the question and ask for the length spectrum as determined by the eigenvalues. For this purpose we consider

$$h(p) \;=\; \cos(pL)e^{-Et} \quad , \quad E = \frac{1}{4} + p^2 \tag{29}$$

which yields the following POSR

$$\begin{aligned} \cosh\frac{L}{2} + \sum_{n=1}^{\infty} d_n \cos(p_n L)e^{-E_n t} \;&=\; 2e^{-\frac{t}{4}} \int_0^\infty dp\, p\, \tanh(\pi p)\cos(pL)e^{-p^2 t} \\ &+\; \frac{e^{-\frac{t}{4}}}{8\sqrt{\pi t}} \sum_{\{l_n\}} \sum_{k=1}^{\infty} \frac{g_n l_n}{\sinh\frac{kl_n}{2}} \left[e^{-\frac{(L-kl_n)^2}{4t}} + e^{-\frac{(L+kl_n)^2}{4t}} \right] \quad . \end{aligned} \tag{30}$$

For $t > 0, L \in \mathbf{R}$, eq.(30) is an exact representation of the *cosine–modulated heat kernel* (compare with eq.(16)). Varying L for fixed but small t, the r.h. side of (30) generates Gaussian peaks of width $\Delta L \sim 2\sqrt{2t}$ exactly at the lengths l_n of the classical periodic orbits. In fig. 8 we show the modulated heat kernel for $t = 0.01$. The full line corresponds to the r.h. side of (30) evaluated with 10000 primitive periodic orbits, whereas the dashed line represents the l.h. side computed from the first 115 eigenvalues. The two curves show for $L > 2.5$ a very similar structure with an equal number of peaks at nearly the same positions. The peaks are less pronounced in the curve computed from the eigenvalues which is not surprising due to the relatively small number of eigenvalues used in the calculation. Nevertheless, one can nicely resolve the lengths l_n of the four shortest primitive periodic orbits having lengths 3.057, 4.897, 5.828 and 6.672, respectively.

The peak near 7.2 corresponds to the two next shortest lengths at 7.107 and 7.263, respectively. Since for $t = 0.01$ the length resolution is only $\Delta L \sim 0.3$, we cannot expect to resolve these two lengths. Above these two lengths up to $L = 9$ there are altogether 8 lengths which, however, overlap appreciably. The two bumps near 8.2 and 8.8 correspond to the two lengths at 8.225 and 8.872 whose multiplicities g_n are 192 and 288, respectively. These multiplicities are much higher than the corresponding average multiplicity which is around 100, and since the two lengths are separated by $\Delta L = 0.65$, they cause the two bumps seen in fig. 8. For $L > 9$ the length spectrum becomes denser and denser according to the law $\Delta L \sim 8\sqrt{2}e^{-L/2}$, and one expects with our resolution a smooth behaviour given by $\cosh(\frac{L}{2})$, the first term on the l.h. side of eq.(30). If the resolution $\Delta L \sim 2\sqrt{2t}$ is improved by making t smaller and smaller, the graph of the modulated heat kernel looks more and more chaotic. Although the lengths themselves obey a simple law, their multiplicities show a very chaotic behaviour with large fluctuations around the average value $\sim 8\sqrt{2}e^{L/2}/L$ as can be seen from fig. 5 and table 1 in [14].

V.8 Periodic–orbit theory with a finite number of lengths

Until now, we only considered sum rules in which infinitely many orbits contribute to the sum, but one can construct sum rules with a finite number of orbits or even without any orbit! This can be achieved by choosing $h(p)$ with a parameter L in such a way, that its Fourier transform $g(x)$ vanishes for $L < l_0$, where l_0 is the shortest length of the length spectrum $\{l_n\}$. Then the sum over the

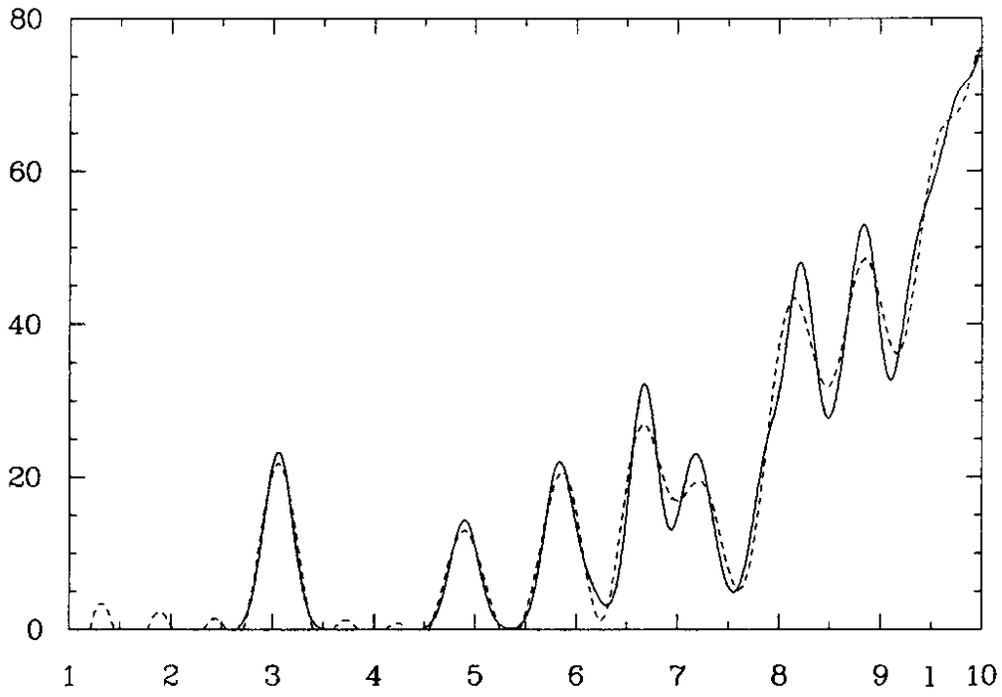

Figure 8: The cosine–modulated heat kernel (30) betrays the length spectrum

length spectrum cannot contribute to the sum rule. Thus one gets a sum rule where the sum over the eigenvalue spectrum is only determined by the integral contribution. Let us first consider

$$h(p) = \left[\frac{N}{pL}\sin\frac{pL}{N}\right]^N \quad , \; N = 3,4,5,\cdots \tag{31}$$

which leads to

$$\left[\frac{2N}{L}\sinh\frac{L}{2N}\right]^N + \left(\frac{N}{L}\right)^N \sum_{n=1}^{\infty} d_n \left[\frac{\sin\frac{p_n L}{N}}{p_n}\right]^N = \tag{32}$$
$$\frac{\text{Area}(F)}{2\pi}\left(\frac{N}{L}\right)^N \int_0^\infty \frac{dp}{p^{N-1}}\tanh(\pi p)\left[\sin\frac{pL}{N}\right]^N + \sum_{\{l_n\}}\sum_{k=1}^{\infty}\frac{g_n\, l_n}{2\sinh\frac{k\, l_n}{2}} g(k\, l_n) \quad .$$

The sum over the length spectrum vanishes for $L < l_0 = 3.057\cdots$ yielding a parameter–free sum rule for the eigenvalues. Remarkably the integral term depends only on the area of the fundamental domain $\text{Area}(F) = 4\pi(g-1)$, where g is the genus. Thus the r.h. side of eq.(32) is the same for all octagons in spite of their different shapes and quantal energies. Only the range of validity depends on the shape which determines the shortest length l_0. We have checked the sum rule and found a nice agreement again.

Another choice for a function $h(p)$ yielding a sharp cut off in the summation over the length spectrum is

$$h(p') = \frac{\sin(L(p'-p))}{p'-p} + \frac{\sin(L(p'+p))}{p'+p} \quad ; \; p' > 0 \, , \; L > 0 \tag{33}$$

which produces the following POSR for $g = 2$:

$$\sum_{n=0}^{\infty}\left[\frac{\sin(L(p_n-p))}{p_n-p} + \frac{\sin(L(p_n+p))}{p_n+p}\right] =$$

$$p\int_{-L}^{L}\frac{\sin(px)}{\sinh\frac{x}{2}}dx + 2\frac{\cos(Lp)}{\sinh\frac{L}{2}} + \sum_{\{l_n\}}\sum_{k=1}^{\infty}\frac{g_n\, l_n}{2\sinh\frac{k\, l_n}{2}}\cos(pkl_n)\Theta\left(L^2-k^2l_n^2\right) \quad . \tag{34}$$

(Here $\Theta(x)$ denotes the Heaviside step function and must not be confused with the heat kernel (16).) Again one has for $L < l_0$ a parameter–free sum rule only for the eigenvalues. If one chooses the parameter L so that one takes into account only the first few lengths one gets a curve with nice peaks in the momentum p but the resolution is very bad if L is too small. One can get peaks resolving the eigenvalues only for very large L, but then the zero mode $E_0 = 0$, i.e. $p_0 = \frac{i}{2}$, causes numerical difficulties, which are absent in the Gaussian–smeared level density, for example. To see this note that the zero mode gives the dominant contribution

$$h\left(\frac{i}{2}\right) = \frac{-2}{E}\left\{\frac{1}{2}\sinh\frac{L}{2}\,\cos(Lp) + p\cosh\frac{L}{2}\,\sin(Lp)\right\}$$

where the amplitudes of the oscillations in p increase exponentially with L. Therefore in order to get information on the eigenvalues $E_n > E_0$ one must subtract two large terms and only the minute difference arises from the eigenvalues $E_n > E_0$.

VI Statistical properties of the energy spectrum

VI.1 Desymmetrization

To study the statistical properties of the energy spectrum in view of a possible signature of quantum chaos one must desymmetrize the system, because one is not interested in correlations of the spectrum due to symmetries.

A look on fig. 9 reveals that the fundamental domain of the regular octagon is mapped onto itself by rotations in steps of $\frac{\pi}{4}$ and by reflections along the symmetry axes (dotted lines in fig. 9). One such reflection and one rotation by $\frac{\pi}{4}$ are the generators of the Dieder–group D_8.

To obtain the eigenvalues for a definite symmetry class, one has to transform the matrices A and B in eq.(11) to a basis of vectors, which belongs to the irreducible representations of the group D_8. In eq.(11) each basis vector describes the values u_i at one point in the finite element mesh. Now the symmetry operations connect those points which can be mapped onto each other by operations of D_8. (These points are indicated by the values $u_1,\ldots,u_{16}$ in fig. 9.) Group theory (see [16]) yields the basis vectors according to the D_8 symmetry which describes the relation of the function values u_i at those 16 points. The basis vectors can be classified in 4 one–dimensional ($\vartheta_1^1,\vartheta_2^1,\vartheta_3^1,\vartheta_4^1$) and 3 two–dimensional ($\vartheta_1^2,\vartheta_2^2,\vartheta_3^2$) representations as listed in table 2. For a one–dimensional representation it suffices to know one of the 16 function values, because then all others can be read off from the basis vectors belonging to the interesting representation. A two–dimensional representation requires two values because there are two basis vectors determining the function values.

Then the transformed matrices A' and B' based on the basis vectors obeying the D_8 symmetry have non–zero elements only in 10 square–submatrices along the diagonal belonging to the different irreducible representations. The large eigenvalue problem seperates so in 10 smaller ones.

An additional difficulty arises from the fact, that the periodic boundary condition requires different mixtures of Dirichlet and Neumann boundary conditions for each group representation, so a general numerical treatment is impossible. To see this, imagine that the points u_1 to u_{16} of fig. 9 lie on the boundary. Then the periodic boundary condition demands for the function values $u_1 = u_{10}$ and $u_2 = u_9$ for example (fig. 9). There are only two representations, ϑ_1^1 and ϑ_3^1, which satisfy these

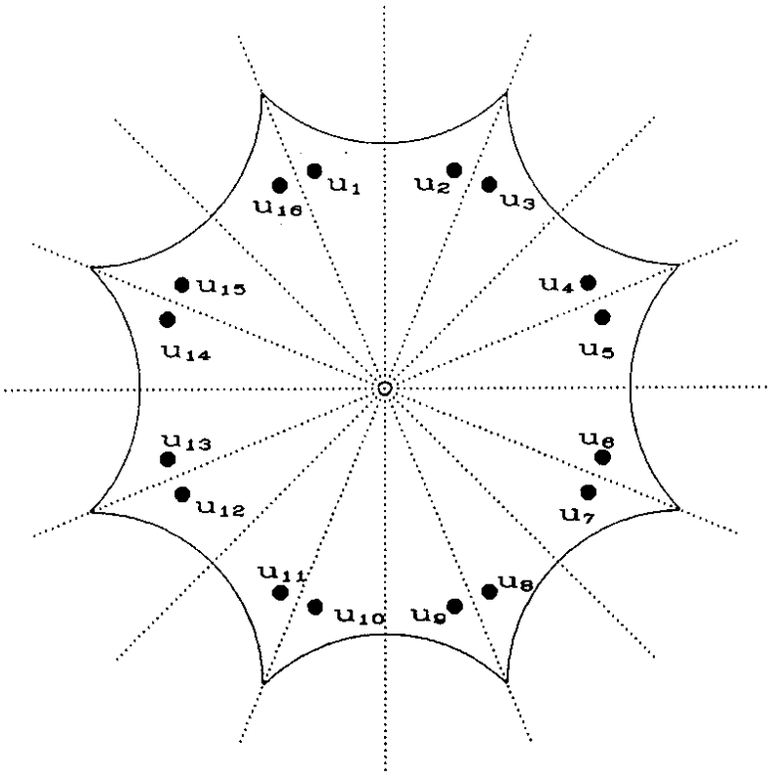

Figure 9: Symmetries in the regular octagon

conditions. All other vectors according to the Dieder D_8 symmetry contradict the periodic boundary condition.

For the representations ϑ_2^1 and ϑ_4^1 one obtaines from table 2 $u_1 = -u_{10}$ and $u_2 = -u_9$, therefore these two representations can be calculated by composing Dirichlet boundary conditions ($u_1 = 0, u_2 = 0, \cdots$).

In contrast for the 3 more complicated two–dimensional representations the additional demand of Dirichlet conditions would yield not a subset of the energy spectrum with periodic boundary conditions, i.e. not a subset of a spectrum of a Riemann surface. In the following we restrict ourselves to the 4 one–dimensional representations.

For these one–dimensional representations it is not necessary to start with the whole matrices A and B for calculating the energy spectrum. It is sufficient to consider the triangle which is enclosed between two adjacent symmetry axes and the boundary. For the 4 one–dimensional representations one has to choose the Neumann and Dirichlet boundary conditions as depicted in fig. 10.

These boundary conditions follow from table 2. For example consider the points u_2 and u_3 in fig. 9, then for $u_2 = u_3$, one has a Neumann boundary condition and for $u_2 = -u_3$ a Dirichlet boundary condition on the dotted symmetry axis between u_2 and u_3.

Expensive computation time can be saved if the method of finite elements is applied directly to the above described triangles with mixed boundary conditions. The 4 energy spectra shown in fig.11 have been calculated again at the HLRZ using the method of finite elements with polynomials of fifth order as ansatz–functions in the triangles. The eigenvalues of the representation ϑ_2^1, i.e. Dirichlet boundaries on all edges, have already been computed by Schmit [17].

VI.2 Level spacing

The main presumption of "quantum chaos" is that all quantum systems, whose classical limit is chaotic, share common statistical properties of their energy spectra, in particular the fluctuations of

	ϑ_1^1	ϑ_2^1	ϑ_3^1	ϑ_4^1	ϑ_l^2		$(l=1,2,3)$	
u_1	1	1	1	-1	1	0	0	-1
u_2	1	-1	1	1	1	0	0	1
u_3	1	1	-1	1	$\cos\frac{\pi l}{4}$	$-\sin\frac{\pi l}{4}$	$\sin\frac{\pi l}{4}$	$-\cos\frac{\pi l}{4}$
u_4	1	-1	-1	-1	$\cos\frac{\pi l}{4}$	$\sin\frac{\pi l}{4}$	$\sin\frac{\pi l}{4}$	$\cos\frac{\pi l}{4}$
u_5	1	1	1	-1	$\cos 2\frac{\pi l}{4}$	$-\sin 2\frac{\pi l}{4}$	$\sin 2\frac{\pi l}{4}$	$-\cos 2\frac{\pi l}{4}$
u_6	1	-1	1	1	$\cos 2\frac{\pi l}{4}$	$\sin 2\frac{\pi l}{4}$	$\sin 2\frac{\pi l}{4}$	$\cos 2\frac{\pi l}{4}$
u_7	1	1	-1	1	$\cos 3\frac{\pi l}{4}$	$-\sin 3\frac{\pi l}{4}$	$\sin 3\frac{\pi l}{4}$	$-\cos 3\frac{\pi l}{4}$
u_8	1	-1	-1	-1	$\cos 3\frac{\pi l}{4}$	$\sin 3\frac{\pi l}{4}$	$\sin 3\frac{\pi l}{4}$	$\cos 3\frac{\pi l}{4}$
u_9	1	1	1	-1	$\cos 4\frac{\pi l}{4}$	$-\sin 4\frac{\pi l}{4}$	$\sin 4\frac{\pi l}{4}$	$-\cos 4\frac{\pi l}{4}$
u_{10}	1	-1	1	1	$\cos 4\frac{\pi l}{4}$	$\sin 4\frac{\pi l}{4}$	$\sin 4\frac{\pi l}{4}$	$\cos 4\frac{\pi l}{4}$
u_{11}	1	1	-1	1	$\cos 5\frac{\pi l}{4}$	$-\sin 5\frac{\pi l}{4}$	$\sin 5\frac{\pi l}{4}$	$-\cos 5\frac{\pi l}{4}$
u_{12}	1	-1	-1	-1	$\cos 5\frac{\pi l}{4}$	$\sin 5\frac{\pi l}{4}$	$\sin 5\frac{\pi l}{4}$	$\cos 5\frac{\pi l}{4}$
u_{13}	1	1	1	-1	$\cos 6\frac{\pi l}{4}$	$-\sin 6\frac{\pi l}{4}$	$\sin 6\frac{\pi l}{4}$	$-\cos 6\frac{\pi l}{4}$
u_{14}	1	-1	1	1	$\cos 6\frac{\pi l}{4}$	$\sin 6\frac{\pi l}{4}$	$\sin 6\frac{\pi l}{4}$	$\cos 6\frac{\pi l}{4}$
u_{15}	1	1	-1	1	$\cos 7\frac{\pi l}{4}$	$-\sin 7\frac{\pi l}{4}$	$\sin 7\frac{\pi l}{4}$	$-\cos 7\frac{\pi l}{4}$
u_{16}	1	-1	-1	-1	$\cos 7\frac{\pi l}{4}$	$\sin 7\frac{\pi l}{4}$	$\sin 7\frac{\pi l}{4}$	$\cos 7\frac{\pi l}{4}$

Table 2: The basis vectors obeying the D_8 symmetry

the levels around the mean level distribution. The two most studied statistics are the level spacing and the spectral rigidity, to which we devote two sections. These statistics should betray a quantum system as a chaotic one.

In integrable quantum systems a Poisson distribution describes the level spacing statistics, whereas for chaotic ones level repulsion is expected, i.e. a distribution vanishing as the level spacing tends to zero. The random matrix theory [18] suggests two different distributions, which are well approximated by

$$P(s) = \frac{\pi}{2} s e^{-\frac{\pi}{4}s^2} \qquad \text{(GOE)} \tag{35}$$

$$P(s) = \frac{32}{\pi^2} s^2 e^{-\frac{4}{\pi}s^2} \qquad \text{(GUE)} \quad , \tag{36}$$

where s is the normalized spacing between two neighbouring levels. The GOE distribution, the so–called Wigner distribution, should be valid for chaotic quantum systems with time reversal symmetry, whereas GUE should apply if the system has no such symmetry. Thus our system is a candidate for the Wigner distribution.

The energy spectra $\{E_i\}$ must be normalized to $\{E_i^n\}$ such that the mean spacing between neighbouring elements is unity. This is achieved by transforming E_i with the aid of Weyl's law $N(E)$ which accounts for the mean trend in the spectrum:

$$E_i^n := N(E_i) \quad . \tag{37}$$

For our 4 one–dimensional representations, Weyl's law can be found as outlined in [13] and one obtains

$$\vartheta_1^1 \quad : \quad N_1(E) = \frac{1}{16}E + \frac{1}{4\pi}(l_0 + \frac{1}{2}l_1)\sqrt{E} + \frac{67}{96} \tag{38}$$

$$\vartheta_2^1 \quad : \quad N_2(E) = \frac{1}{16}E - \frac{1}{4\pi}(l_0 + \frac{1}{2}l_1)\sqrt{E} + \frac{67}{96} \tag{39}$$

$$\vartheta_3^1 \quad : \quad N_3(E) = \frac{1}{16}E + \frac{1}{4\pi}(l_0 - \frac{1}{2}l_1)\sqrt{E} \tag{40}$$

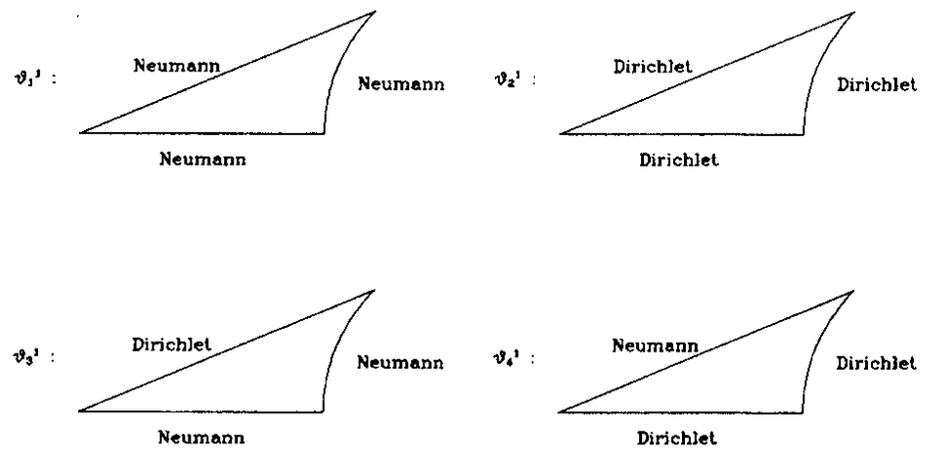

Figure 10: Boundary conditions for the one–dimensional representations

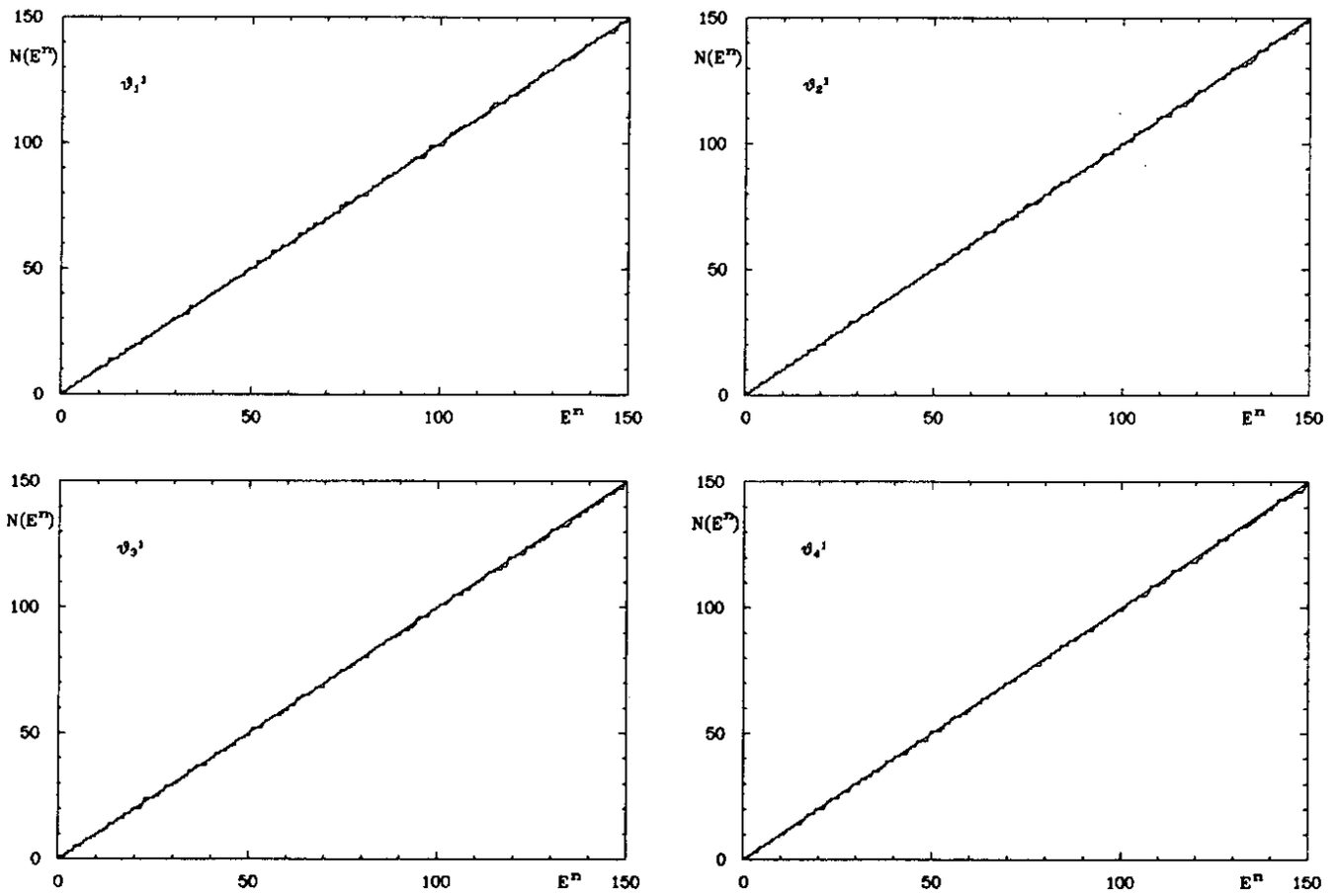

Figure 11: Normalized spectra of the 4 one–dimensional representations in comparison with Weyl's law

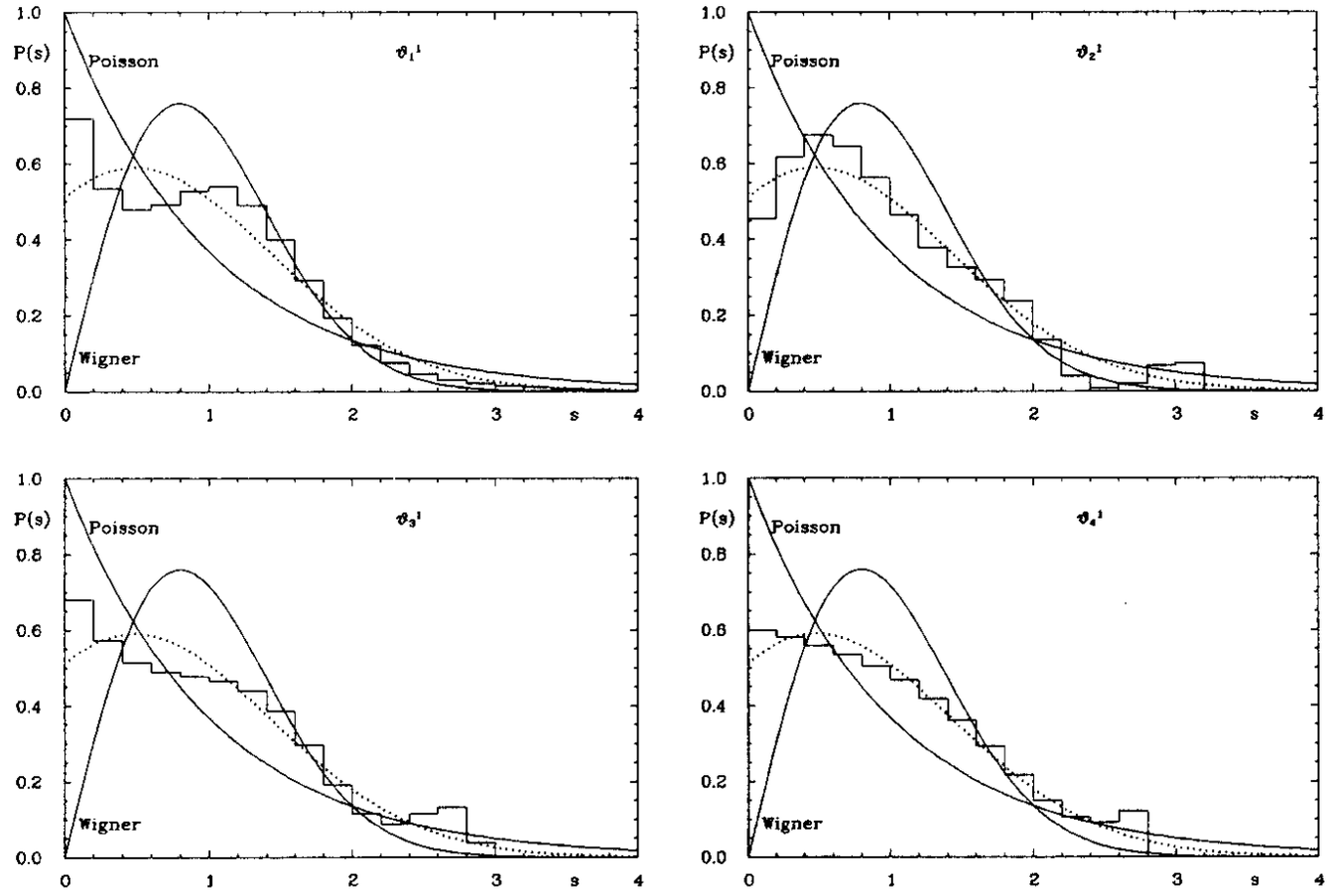

Figure 12: Level spacing of the 4 one–dimensional representations in comparison with various theoretical distributions as explained in the text. The dotted curve is the Berry–Robnik distribution eq.(42) for $\rho = 0.3$.

$$\vartheta_4^1 \quad : \quad N_4(E) \;=\; \frac{1}{16}E - \frac{1}{4\pi}(l_0 - \frac{1}{2}l_1)\sqrt{E} \quad . \tag{41}$$

Here l_0 and l_1 are the lengths of the two shortest classical periodic orbits of the symmetrical Hadamard–Gutzwiller model. Weyl's law for the normalized spectra $\{E_i^n\}$ reads now $N(E^n) \sim E^n, E^n \to \infty$, of course. These spectra are shown in fig. 11 in comparison with Weyl's law, where one observes an excellent match for the first 140 eigenvalues. The eigenvalues above $E^n \simeq 140$ are somewhat too large and therefore lead to a staircase $N(E)$ lying slightly under Weyl's law. This is a consquence of the method of finite elements, because it is based on a variational principle yielding upper bounds for the eigenvalues which are, however, for the first 125 eigenvalues very good approximations to the true eigenvalues. Only these first 125 eigenvalues are used in the following statistical considerations. We use a smoothing procedure for the histograms because otherwise large fluctuations in the bins would hide the true statistical behaviour. This procedure smoothes a distribution by carrying out a Fourier synthesis of the damped power spectrum obtained from a Fourier analysis of the given distribution.

Fig. 12 shows the smoothed level spacing distributions for the 4 one–dimensional representations in comparison with the Poisson and Wigner distribution. Neither of them agrees with our results, whereas the dotted line gives a reasonable fit. It corresponds to a superposition of a Poisson and

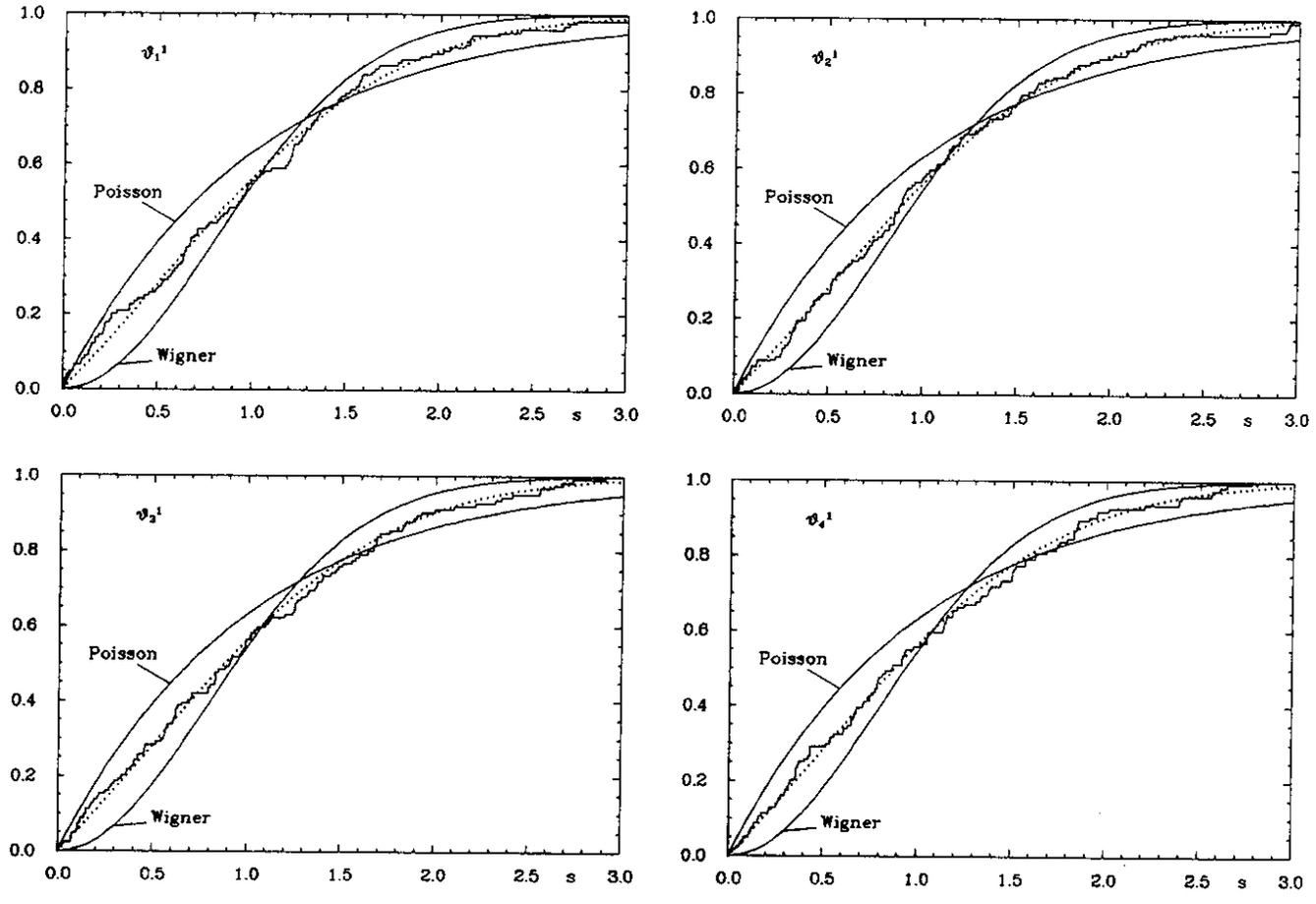

Figure 13: Cumulative level spacing $\int_0^s P(s')\,ds'$ for the 4 one–dimensional representations in comparison with various theoretical distributions as explained in the text

Wigner distribution as proposed by Berry and Robnik [19]:

$$P(s,\rho) = \rho^2 e^{-\rho s}\mathrm{erfc}(\frac{\sqrt{\pi}}{2}\bar{\rho}s) + \left(2\rho\bar{\rho} + \frac{\pi}{2}\bar{\rho}^3 s\right) e^{-\rho s - \frac{\pi}{4}\bar{\rho}^2 s^2} \quad ; \quad \bar{\rho} = 1 - \rho \tag{42}$$

for $\rho = 0.3$. [1] To avoid the smoothing procedure, let us consider the *cumulative level spacing*

$$\int_0^s P(s')\,ds' \quad , \tag{43}$$

which yields a useful statistics even for a relatively small sample of level spacings. The result is presented in fig. 13 where the staircase function $\int_0^s P(s')\,ds'$ is shown in comparison with the cumulative Poisson and Wigner distributions. Again neither of them agrees well with the staircase. A much better match is obtained for the cumulative "Berry–Robnik distribution" using $\rho = 0.3$ (dotted line in fig. 13).

Thus our results don't support the hypothesis that chaotic quantum systems with time reversal symmetry should display a pure Wigner distribution. Rather our systems behave as if their phase spaces were divided in chaotic and integrable regions. Following random matrix theory one would

[1] The parameter ρ measures the integrable contribution, if one identifies the integrable contribution with the Poisson distribution.

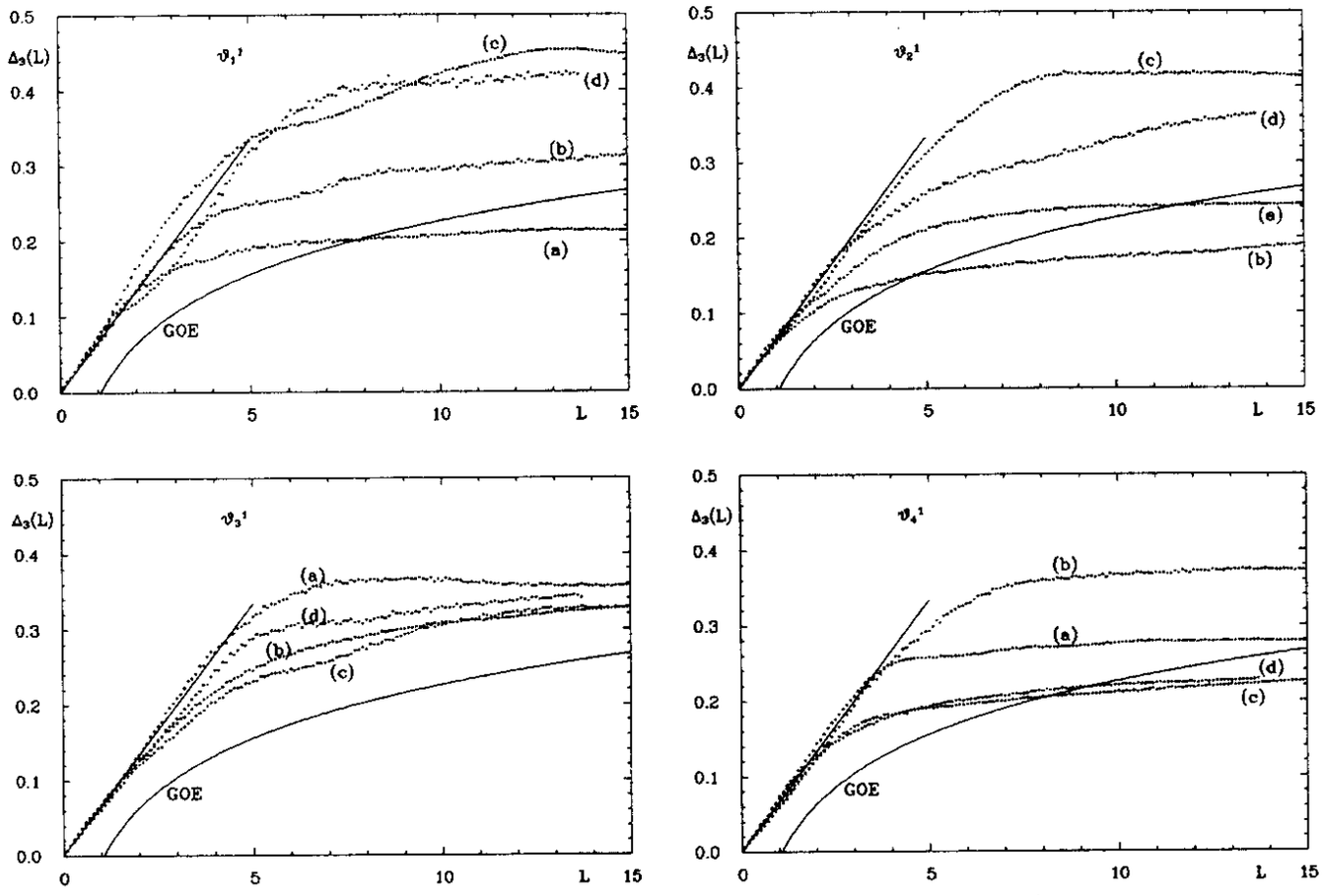

Figure 14: The spectral rigidity is shown for 4 distinct energy ranges : for E=30 (a), E=50 (b), E=70 (c) and E=90 (d). The straight line has a slope of $\frac{1}{15}$.

come to the conclusion that our systems are chaotic to only 70%, even though we know that they are purely chaotic. We would like to emphasize that the symmetry cannot be called for to account for this result, because we desymmetrized the regular octagon in irreducible representations according to group theory. Perhaps the random matrix theory should be weakened to the statement that chaotic systems never display a pure Poisson distribution.

It is notoriously difficult to compute more than a few hundred eigenvalues up from the ground state numerically for non–integrable systems, and there arises another possiblity for the flaw in our statistics which lies beyond our power of judgment, because it could be, that the semiclassical properties are not valid in the low energy range which we doomed to use. However the practice often shows that semiclassical approximations like WKB describe many systems well up to the low energy range. So it can be hoped that the behaviour of our system varies only slightly over the energy scale, too.

VI.3 Spectral rigidity

The spectral rigidity $\Delta_3(L)$ measures the fluctuations of the spectrum over an energy range corresponding to L mean level spacings, whereas the level spacing itself only measures the fluctuations between two neighbouring levels. The rigidity $\Delta_3(L)$ was defined in [20] as the average of the mean

square deviation of the staircase $N(E)$ from the best fitting straight line $a + b\varepsilon$:

$$\Delta_3(L) := \left\langle \min_{(a,b)} \frac{1}{L} \int_{-L/2}^{L/2} d\varepsilon \, [N(E+\varepsilon) - a - b\varepsilon]^2 \right\rangle \tag{44}$$

where $< >$ denotes a local average. The constants a and b can be eliminated yielding

$$\Delta_3(L) = \left\langle \frac{1}{L} \int_{-L/2}^{L/2} d\varepsilon N^2(E+\varepsilon) - \left[\frac{1}{L} \int_{-L/2}^{L/2} d\varepsilon N(E+\varepsilon) \right]^2 - 12 \left[\frac{1}{L^2} \int_{-L/2}^{L/2} d\varepsilon \varepsilon N(E+\varepsilon) \right]^2 \right\rangle \quad . \tag{45}$$

The behaviour of the spectral rigidity depends on the statistical properties of the underlying spectrum, of course. Only the behaviour for $L << 1$, where $\Delta_3(L) \sim \frac{1}{15} L$, and the fact that $\Delta_3(L)$ tends to a non–universal saturation value Δ_∞ for large L is independent of the underlying spectrum. Therefore most important is the transition region for which the random matrix theory asserts for GOE

$$\Delta_3(L) \sim \frac{1}{\pi^2} \ln L + \text{ const} \tag{46}$$

with const = -0.00695. In contrast to the level spacing there exists a semiclassical theory for $\Delta_3(L)$ which was developed in [21]. For chaotic systems with time reversal symmetry this theory predicts the same behaviour for $\Delta_3(L)$ as the GOE–theory. An integrable system continues to display the low–L behaviour even in the transition region, i.e. $\Delta_3(L) \sim \frac{1}{15} L$ and then turns over to a non–universal saturation value Δ_∞.

In fig. 14 the rigidity is shown for the 4 one–dimensional symmetry classes. The rigidity is calculated for the four energies $E^n = 30$, $E^n = 50$, $E^n = 70$ and $E^n = 90$,respectively. The local average $< >$ in eq.(45) is obtained by averaging in the interval $[E^n - \delta E, E^n + \delta E]$ where we use $\delta E = 10$. For all classes we observe good agreement with a straight line with slope $\frac{1}{15}$ in the interval $0 < L < 2$. Beyond this universality region one observes a very strong dependence on the energy, which is caused by the very small averaging interval. Because of lack of more eigenvalues, we have no other choice. The energy dependence is too strong to observe a universality like the GOE prediction (46), which is shown in fig. 14 too.

VII Summary

In this paper we have presented a rigorous approach to quantum chaology of spectra for an ergodic system, the Hadamard–Gutzwiller model. This model is a Hamiltonian system of two degrees of freedom which describes the geodesic flow on a surface of constant negative curvature. Our approach has been based on the *Selberg trace formula* (13) which yields infinitely many POSRs. These sum rules establish a striking and "apparently paradoxical" duality relation between the *quantal* energy spectrum $\{E_n\}$ and the length spectrum $\{l_n\}$ of *classical* periodic orbits. One has thus found an exact substitute, appropriate for our strongly chaotic system, for the Bohr–Sommerfeld–Einstein quantization rules. A main purpose of this paper has been to demonstrate that PO theory provides a practical tool for quantum chaology which even allows to calculate spectra. Finally, we have studied the level spacing and the spectral rigidity for 4 desymmetrized subspectra of the symmetrical Hadamard–Gutzwiller model.

Acknowledgement

We would like to thank the Deutsche Forschungsgemeinschaft for financial support and the HLRZ at Jülich for the access to the CRAY–XMP computer.

References

[1] M.V.Berry, Proc. Roy. Soc. London, Ser. **A413**(1987) 183.

[2] A.Einstein, Verh. Dtsch. Phys. Ges. **19**(1917) 82.

[3] M.C.Gutzwiller, J.Math.Phys. **8**(1967) 1979 ; ibid. **10** (1969) 1004 ; ibid. **11**(1970) 1791; ibid. **12**(1971) 343; in *Path Integrals and their Applications in Quantum, Statistical and Solid-State Physics*, edited by G.J.Papadopoulos and J.T.Devreese (Plenum,New York, 1978), p.163 .

[4] R.Balian and C.Bloch, Ann. Phys. (NY)**69**(1972) 76 ; ibid. **85**(1974) 514.

[5] R.Dashen, B.Hasslacher and A.Neveu, Phys.Rev. **D10**(1974) 4114.

[6] M.V.Berry, in *Semiclassical Mechanics of Regular and Irregular Motion*, Proceedings of the Les Houches Summer School, Section XXXVI, edited by G.Iooss, R.H.G.Helleman and R.Stora (North-Holland,Amsterdam, 1983), p.171 .

[7] M.Sieber and F.Steiner, DESY preprint, DESY 89-003 (January 1989), submitted to Phys. Rev. Letters.

[8] J.Hadamard, J.de Math. pure et appl. **4**(1898) 27.

[9] M.C.Gutzwiller, Phys. Rev. Letters **45**(1980) 150 ; Physica Scripta **T9**(1985) 184; Contemp. Math. **53**(1986) 215.

[10] A.Selberg, J.Indian Math. Soc. **20**(1956) 47.

[11] F.Steiner, Phys. Letters **B188**(1987) 447.

[12] R.Aurich, M.Sieber and F.Steiner, Phys.Rev.Letters **61**(1988) 483.

[13] N.L.Balazs and A.Voros, Phys. Rep. **143**(1986) 109.

[14] R.Aurich and F.Steiner , Physica **D32**(1988) 451.

[15] H.Huber , Math. Ann. **138**(1959) 1.

[16] E.Stiefel and A.Fässler , Gruppentheoretische Methoden und ihre Anwendungen , Teubner , Stuttgart , 1979.

[17] O.Bohigas, M.-J.Giannoni and C.Schmit , Spectral fluctuations of classically chaotic quantum systems, in: Springer Lecture Notes in Physics **263**(1986).

[18] M.L.Metha, Random matrices and the statistical theory of energy levels, Academic Press, New York, 1967.

[19] M.V.Berry and M.Robnik , J.Phys.A.(Math.Gen.) **17**(1984) 2413.

[20] F.J.Dyson and M.L.Metha , J.Math.Phys. **4**(1963) 701.

[21] M.V.Berry, Proc. Roy. Soc. London, Ser.**A400**(1985) 229.